Impurity Transport Study with TESPEL Injection and Simulation*)

Shigeru SUDO, Naoki TAMURA, Hisamichi FUNABA, Sadatsugu MUTO, Chihiro SUZUKI and Izumi MURAKAMI

National Institute for Fusion Science, 322-6 Oroshi-cho, Toki 509-5292, Japan

(Received 29 November 2012 / Accepted 26 March 2013)

Impurity behaviors in LHD are studied by a Tracer-encapsulated Solid Pellet (TESPEL) injection. By containing multiple tracers in a TESPEL, the different tracer species have been compared simultaneously under the same plasma condition. The density disturbance on the bulk plasma by TESPEL is typically less than 10 %. The amount of the tracer particles deposited locally inside a plasma is about a few 10^{17} particles which is smaller than that of the bulk plasma by a factor of three orders of magnitude. Triple tracers, V, Mn and Co are used, because the charges of nuclei of intrinsic impurities, Cr and Fe are in between those of the tracers. The impurity confinement behavior depends substantially on the electron density. In case of the density higher than $n_e = 5 \times 10^{19}\,m^{-3}$, the tracer impurity in the plasma core was kept for a long time, while it decays in order of 500 ms in the medium density case. Such temporal behavior is compared with a STRAHL simulation code assuming diffusion coefficient and convection. The general behavior fits well with the emissivity value integrated along the sight line.

Keywords: TESPEL, pellet, tracer, impurity diagnostics, impurity transport

DOI: 10.1585/pfr.8.2402059

1. Introduction

Impurity behaviors in LHD are studied by a Tracer-encapsulated Solid Pellet (TESPEL) injection [1–4]. TESPEL consists of polystyrene (polymer in the form of $(C_8H_8)_n$) as an outer shell, and tracers inside of the polystyrene ball with the void of the typical diameter of 250 μm. By containing multiple tracers in a TESPEL, the different tracer species have been compared simultaneously under the same plasma condition [5]. As the diameter of TESPEL is about 700 μm, the density disturbance on the bulk plasma is typically less than 10%. For investigating the impurity transport, we compare the experimental data with the STRAHL [6] code, and describe the general feature of the impurity transport in LHD.

2. Experimental Condition

In case of the TESPEL with outer diameter of 720 μm (in the shot number of #106986), the polystyrene shell contains C and H with the same amount of about 1×10^{19} particles, which corresponds to the total electron number of 7×10^{19}. As the total volume of LHD is $30\,m^3$, the electron density increase by TESPEL injection is about $2 \times 10^{18}\,m^{-3}$ in average. This increase of the density is consistent with the measurement by a Thomson scattering system [7] and a far infrared (FIR) laser interferometer system [8]. So, the density increase by TESPEL is relatively small disturbance to the bulk plasma. This paper treats the two density categories, namely the average density of $3.4 \times 10^{19}\,m^{-3}$ for the medium density case, and $6.6 \times 10^{19}\,m^{-3}$ for the high density case. These parameters on the $n_e - T_e$ diagram are shown in Fig. 1 together with the previous study [9]. The previous study mainly based on the intrinsic impurity such as Fe showed the impurity transport property depends on the collisionality, that is, impurities are accumulated in the Plateau regime, while they are not accumulated in the low and high collisionality regimes. The present study focuses on the impurity transport property of the Plateau and high collisionality regimes, with utilizing triple tracers, V (Z = 23), Mn (Z = 25) and Co (Z = 27). The amount of the tracer particles deposited locally (typically at $\rho \sim 0.6$ - 0.7, where ρ denotes the normalized radius with the outermost radius) inside a plasma is about a few 10^{17} particles which is smaller than that of the bulk plasma by a factor of three orders of magnitude. Under such relatively small disturbance from both the outer shell and tracers to the bulk plasma, the impurity transport property has been investigated with observing Kα emission from the tracers by a soft X-ray pulse height analysis system [10] and line emission from the Li-like ions of the tracers by a SOXMOS spectrometer system in the vacuum ultra violet regime [11]. These lines are integrated ones from the plasma along the sight line of the detectors. In order to analyze the experimental data, the time dependent

author's e-mail: sudo@nifs.ac.jp

*) This article is based on the presentation at the 22nd International Toki Conference (ITC22).

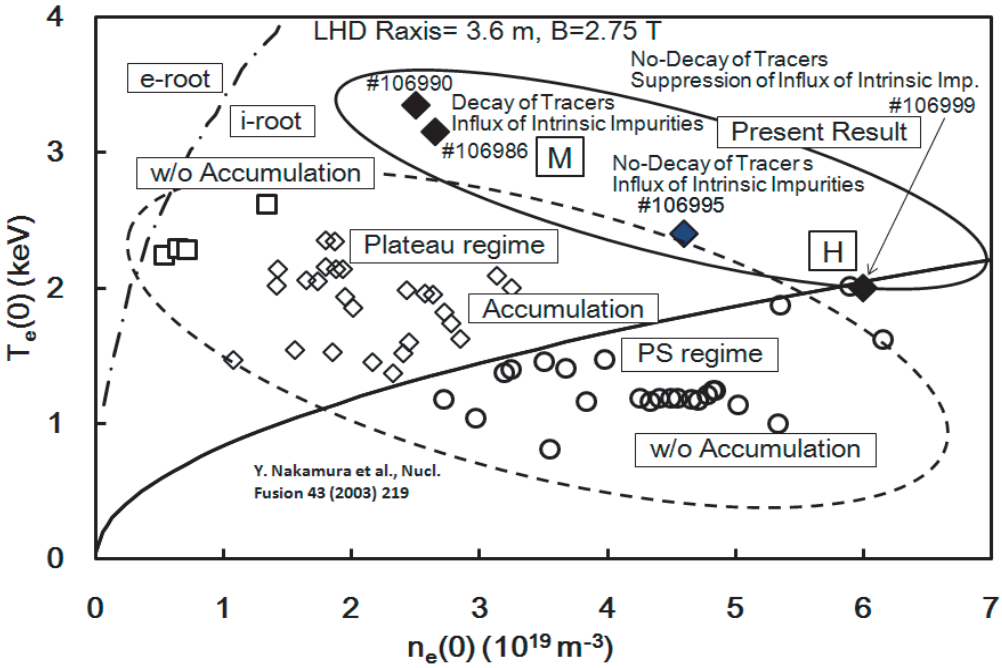

Fig. 1 Regime of impurity transport study on $n_e - T_e$ diagram. The high density case: H and medium density case: M described in this paper are also shown in the figure.

STRAHL code is used with assuming the diffusion coefficient and the convection velocity in the impurity transport equation. And, the local calculated emissivity is integrated along the sight line of the experimental condition to compare with the experimental data.

3. Comparison of Experimental Data with STRAHL Simulation

In order to analyze the experimental data, one dimensional impurity transport code, STRAHL is used for calculating the charge state densities and emission line intensities of the impurity ions. It has an advantage of using the atomic data from ADAS (Atomic Data and Analysis Structure) [12] easily.

The impurity transport equation is:

$$\frac{\partial n_{I,Z}}{\partial t} = \frac{1}{r}\frac{\partial}{\partial r} r\left(D_{I,Z}\frac{\partial n_{I,Z}}{\partial r} - V_{I,Z} n_{I,Z}\right) + Q_{I,Z},$$

where $n_{I,Z}$ is the charge state density of species I and charge state Z, and the $D_{I,Z}$ and $V_{I,Z}$ are diffusion coefficient and convection velocity. $Q_{I,Z}$ denotes source and sink term due to ionization and recombination.

The present study assumes diffusion coefficient and convection velocity are the same for all charge states and species, namely $D_{I,Z} = D$ and $V_{I,Z} = V$.

In this series of experiments, V, Mn and Co are used as tracers in the LHD plasmas as stated in the previous section. The calculated temporal evolutions of the Li-like and He-like charge state densities of V in the high density case (6.6×10^{19} m^{-3}) are shown in Fig. 2. These show the peak started at the location of the tracer deposition ($\rho \sim 0.61$)

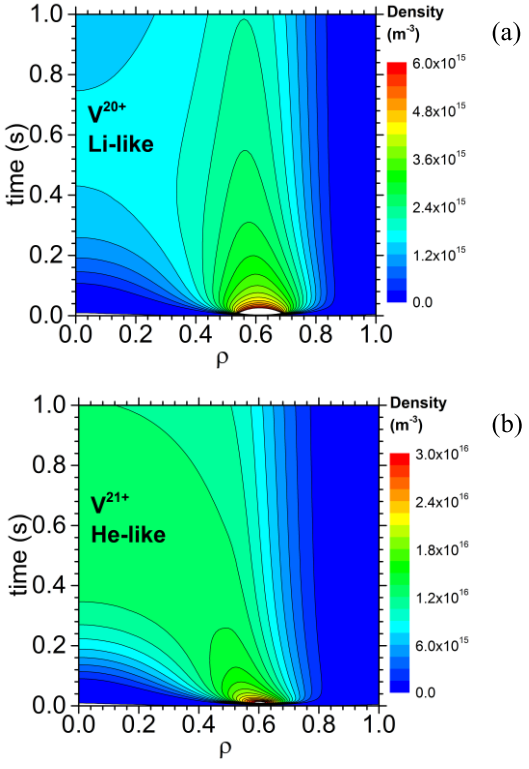

Fig. 2 The temporal evolution of (a) Li-like and (b) He-like charge states of V calculated by STRAHL in the high density case.

and it moved inward to the center in case of V^{21+} (He-like charge state). In contrast to this, the location of the peak of V^{20+} (Li-like charge state) moved inward only slightly

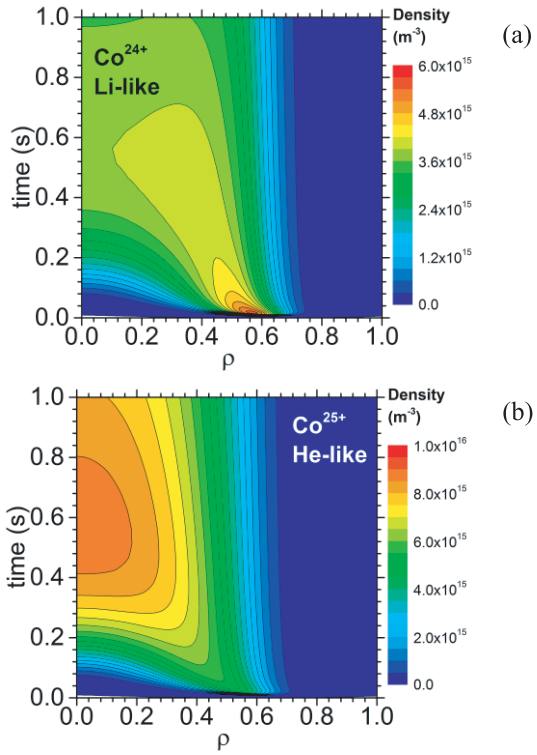

Fig. 3 The temporal evolution of (a) Li-like and (b) He-like charge states of Co calculated by STRAHL in the high density case.

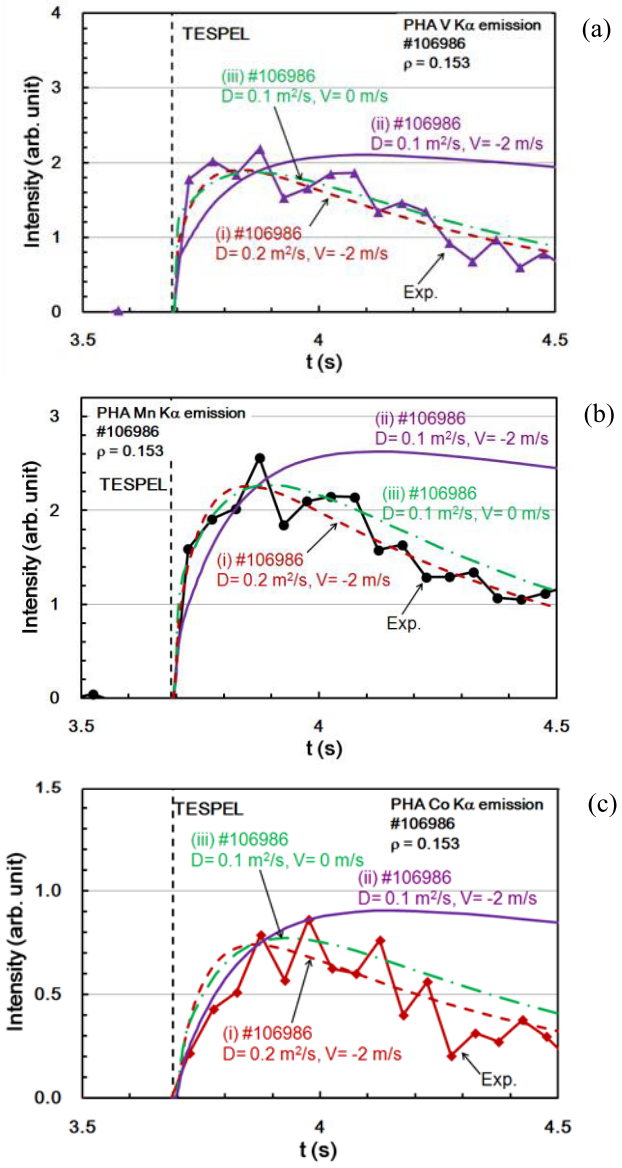

Fig. 4 The temporal evolution of the experimentally observed Kα line emissions of V, Mn and Co for the medium density case. The emissivity integrated along the line of sight calculated by STRAHL with three different sets of D and V is also shown.

in the initial phase and then it was remaining at the same location. This is due to the rapid ionization of V^{20+} to the higher charge state in the inner plasma region where T_e is higher than the initial location of the tracer deposition. Here, the impurity diffusion coefficient D is assumed as 0.1 m^2/s (spatially constant), and the convection velocity V is assumed as -2 m/s (at $\rho = 0.9$), 0 m/s at $\rho = 0.5$ and $\rho = 1.0$, and these are linearly connected. The negative sign of V means inward convection. The temporal evolutions of Co^{24+} (Li-like charge state) and Co^{25+} (He-like charge state) with the same D and V as in Fig. 2 are shown in Fig. 3. The peak of Co^{24+} and Co^{25+} started at the location of the tracer deposition and it moved inward to the center. These are ion charge state distributions. The STRAHL code can calculate also the emissivity of each line emission. For comparison with the experimental observation, the calculated emissivity is integrated along the corresponding sight line. The result for Kα lines of V, Mn and Co (5.0 keV, 5.9 keV and 6.9 keV for V, Mn and Co, respectively) is shown in Fig. 4 for the medium density case (#106986). The solid lines with symbols denote the experimental data, and the other lines denote the simulated data for the cases (i) $D = 0.2$ m^2/s and $V_0 = -2$ m/s (we define V_0 as V at $\rho = 0.9$), (ii) $D = 0.1$ m^2/s and $V_0 = -2$ m/s, (iii) $D = 0.1$ m^2/s and $V_0 = 0$ m/s for the medium density case (in the figure, V means V_0). The intensity is normalized at $t = 3.87$ s for comparing the feature of temporal evolution. The case (i) fits well with the experimental data, while both the rise-up phase and decay phase in case (ii) do not fit with the experimental data. The case (iii) fits well also with the experimental data.

The STRAHL calculation results of Kα emissions of V, Mn and Co with (ii) $D = 0.1$ m^2/s and $V_0 = -2$ m/s are shown in Fig. 5 for the high density case (#106999). Both the rise-up feature in the initial phase and the feature in the later phase ($t = 4.0$ - 4.5 s) of the simulation fit well with the experimental observation within the accuracy. Therefore, the further adjustment of the D and V values is not necessary. For the medium density case, both combinations of (i) $D = 0.2$ m^2/s and $V_0 = -2$ m/s and (iii) $D = 0.1$ m^2/s and $V_0 = 0$ m/s fit well with the experimental data. On the other hand, we did not see any difference in the poloidal

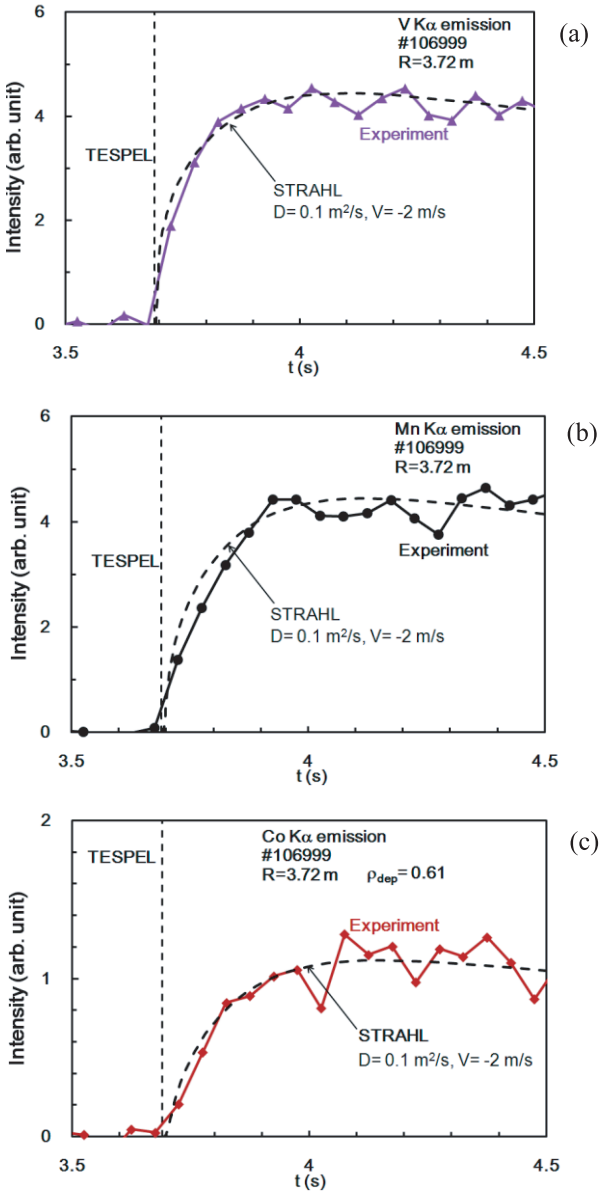

Fig. 5 The temporal evolution of the experimentally observed Kα line emissions of V, Mn and Co and the STRAHL simulation for $D = 0.1\,\mathrm{m^2/s}$ and $V_0 = -2\,\mathrm{m/s}$ for the high density case.

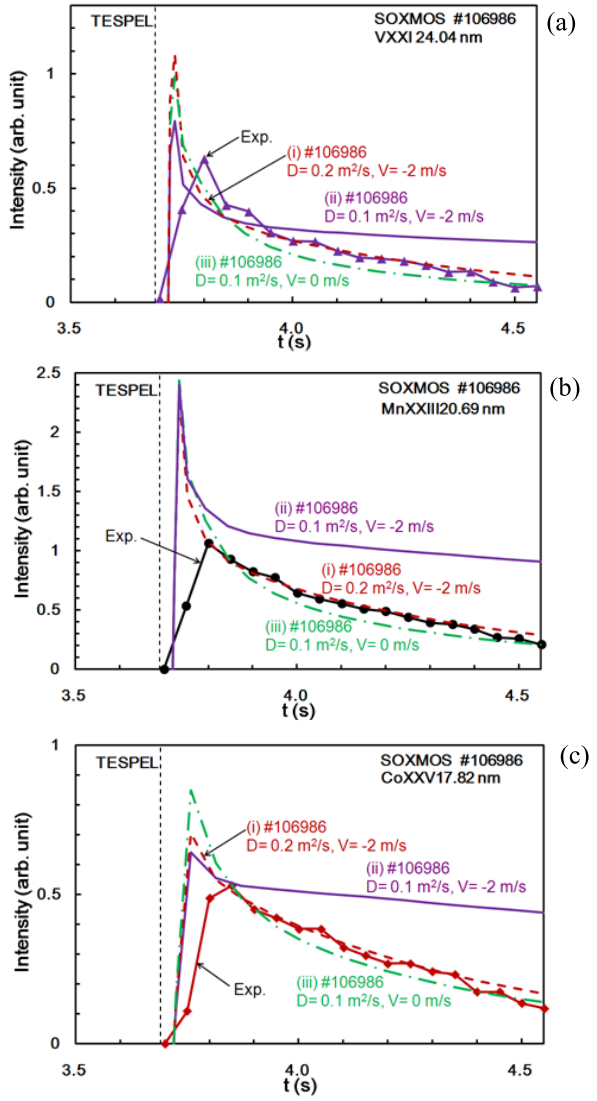

Fig. 6 The comparison of the experimental observation with the STRAHL simulation results for Li-like emissions in the medium density case.

rotation velocity profile for the high and medium density cases in the previous study [5]. And, there is an idea that the dominant driving force for the convection velocity is the radial electric field E_r [13]. The radial electric field is mainly determined with the poloidal rotation velocity V_θ through the relation of $E_r = -V_\theta \times B_\phi$, where B_ϕ is the toroidal component of the magnetic field. Thus, there is no essential difference in E_r for the high and medium density case. From these viewpoints, we take the same V value for the high and medium density cases. In this case, there is a difference with a factor of 2 in D for the high and medium density cases ($D = 0.1\,\mathrm{m^2/s}$ for the high density case and $0.2\,\mathrm{m^2/s}$ for the medium density case, respectively). However, we should note that the idea that the dominant driving force for the convection velocity is the radial electric field is not verified to be applicable in our present case. Thus, the possibility of a change in convection velocity is not yet excluded.

The impurity diffusion coefficient D may be even smaller than $0.1\,\mathrm{m^2/s}$ for the high density case, but for determining this accurately, experiments with longer pulse duration are necessary.

The intensity ratio of Kα lines of the tracers fits also well (assuming that the sensitivity of the detector on the photon energy is the same). As the known tracer amount is an input parameter to the STRAHL code, the good agreement on the intensity ratio of Kα emission for tracers between the experiment and the STRAHL calculation shows the credibility of the emissivity data of ADAS.

The STRAHL calculation results of V, Mn and Co Li-like emissions: 2s-2p (J: 1/2-3/2): 20.69 nm, 24.04 nm and

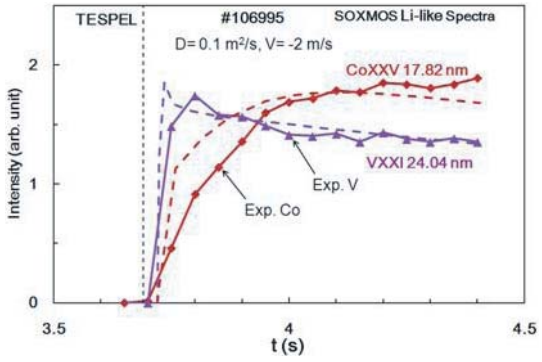

Fig. 7 The comparison of the experimental observation with the STRAHL simulation results for V and Co Li-like emissions in the high density case.

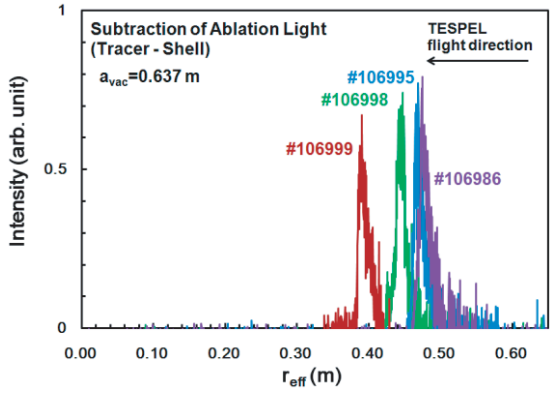

Fig. 8 The tracer source locations for various TESPEL injection shots.

17.82 nm are shown in Figs. 6 (a), (b) and (c), respectively for the medium density case. The three different sets of D and V combination: (i) $D = 0.2\,\mathrm{m^2/s}$ and $V_0 = -2\,\mathrm{m/s}$, (ii) $D = 0.1\,\mathrm{m^2/s}$ and $V_0 = -2\,\mathrm{m/s}$, (iii) $D = 0.1\,\mathrm{m^2/s}$ and $V_0 = 0\,\mathrm{m/s}$ are shown. The experimental data is also shown. The rise-up phase is not affected by the change of combination of D and V in the present range. This is because the Li-like ion is easily ionized to the higher charge state in the initial phase (corresponding to the location near the tracer deposition). This situation is easily understandable from the Li-like ion charge state distribution as shown in Figs. 2 (a) and 3 (a). Thus, the rise-up phase is dominated mainly by the atomic process, not by the transport. In Fig. 7, the STRAHL simulation results of the V and Co Li-like emissions are shown with the experimental data for the high density case. The case of (ii) $D = 0.1\,\mathrm{m^2/s}$ and $V_0 = -2\,\mathrm{m/s}$ fits well with the experimental data in the decay phase. But, there is still some discrepancy in the rise-up phase, which is considered due to the reason as stated above. Here, we should note that the time resolution of the Li-like ion emission (SOXMOS) and Kα emission (PHA) is 50 ms, while the time resolution of STRAHL is auto-adjusted and very high (less than 1 ms) in the initial phase because of the transient phase (starting from the neutral state). Also in the STRAHL simulation, the local effect of the TESPEL ablation on the bulk plasma is not included, so the T_e and n_e of the bulk plasma are taken as constant. From these reasons, there is some limitation to compare the initial phase of the experimentally observed Li-like ion emissions with the present STRAHL calculation, and thus the comparison in only the decay phase (t = 3.9 - 4.5 s) would be meaningful.

Here, we would like to describe about the effect of the penetration depth of the tracers on the impurity behavior. In Fig. 8, the signal from the light through the V I line filter subtracted from that of Hα line filter is shown. This subtraction is made because the signal from the light through the V I line filter is affected by the strong background emission due to the finite bandwidth of the filter, as already stated in the previous paper [5]. The TESPEL injection line is approximately on the elongated direction of the plasma cross section of the equatorial plane. For reference, the magnetic axis R_{ax} in the vacuum condition is 3.60 m, and the outermost radius R_{VAC} of the nested magnetic surface in the vacuum condition is 4.45 m.

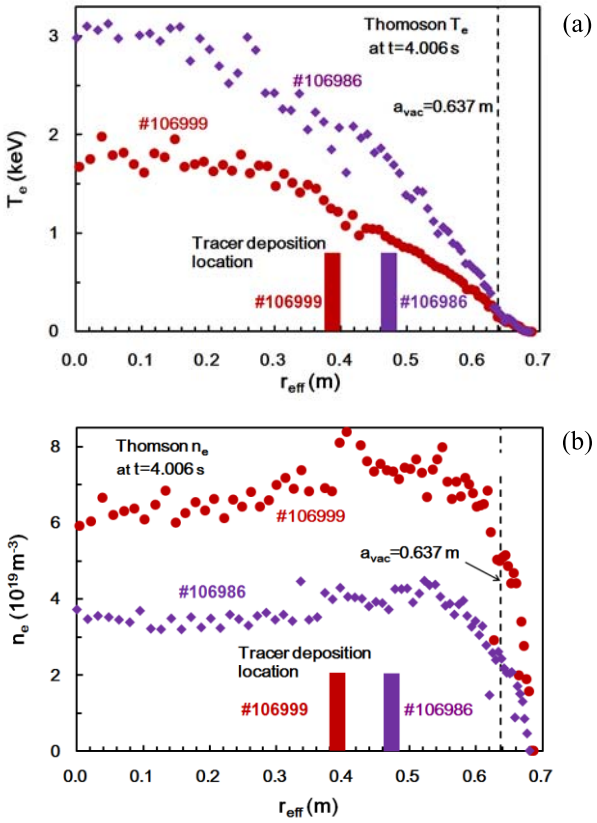

Fig. 9 The electron temperature and density profiles for #106986 and #106999 at t = 4.006 s. The tracer source locations are also indicted with rectangles.

The original major radius is converted to the effective radius, r_{eff} which is defined by a radius corresponding to the constant volume in a cylindrical approximation enclosed by each radial magnetic surface of the real plasma. The r_{eff} is calculated with the equilibrium code includ-

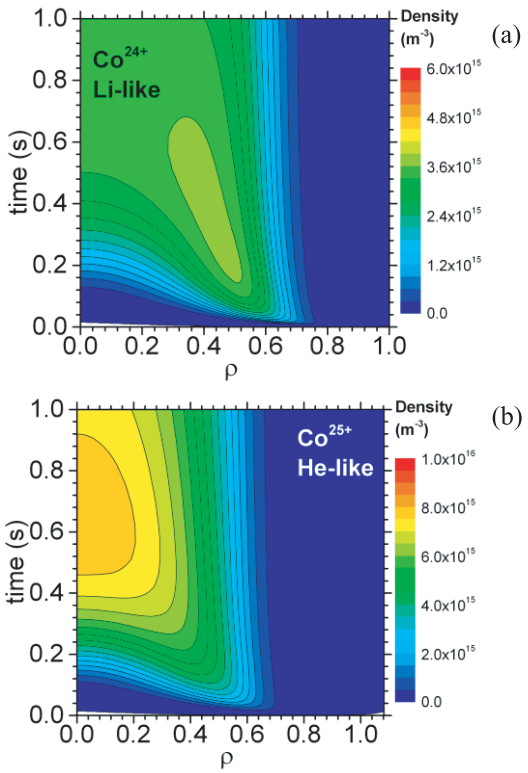

Fig. 10 The Co (a) Li-like and (b) He-like Kα ion charge states in the high density case, but intentionally assumed as the same deposition location of tracers as the medium density case (#106986).

ing the effect of finite beta value. The shots of #106995, #106998 and #106999 show the same property of the "high density case". The variation is due to the slight difference of the TESPEL size and the plasma parameters. And, the shot of #106986 shows the property of the "medium density case". In the "medium density case", the electron temperature becomes higher, thus the penetration tends to be shallower. The electron temperature and density profiles for #106986 and #106999 at $t = 4.006$ s are shown in Fig. 9. The tracer source locations are also indicated with rectangles. The STRAHL calculated Co (a) Li-like and (b) He-like ion charge states in the high density case (#106999), but intentionally assumed as the same deposition location of tracers as the medium density case (#106986) are shown in Fig. 10. This is done for seeing the sensitivity of the deposition location on the impurity transport feature. The Co (a) Li-like and (b) He-like ion charge states in case of the real deposition location of tracers (#106999) are already shown in Fig. 3. Of course, the feature in the initial phase is different in the two cases because of the different deposition location. But, the feature in the later phase resembles with each other. The STRAHL calculation of temporal evolution of Co Kα line emission integrated in the line of sight is shown in Fig. 11. Here, the time $t = 0$ s corresponds to the tracer deposition timing. As shown in the figure, the rise-up of the case of the shallow penetration ($\rho_{\rm dep} = 0.75$,

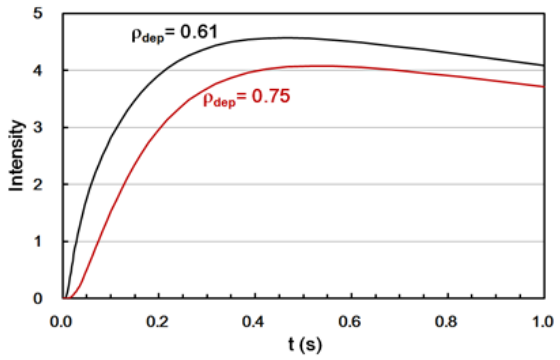

Fig. 11 The STRAHL calculation of the temporal evolution of Co Kα line emission in the high density case.

$\rho_{\rm dep}$ is the deposition location of the tracer normalized by the plasma radius) is, of course, delayed compared to the case of the deeper penetration ($\rho_{\rm dep} = 0.61$), but in the decay phase ($t = 0.4$ - 1.0 s) the temporal behavior is essentially the same for the both cases. As a result, the effect of the different deposited location of the tracer is not sensitive on the impurity behavior.

As for the other viewpoint, the difference between #106995 and #106986 is only a few cm in the elongated direction of the plasma as shown in Fig. 8. As this is only a few % of the whole plasma radius, such difference of the penetration depth doesn't seem essential for determining drastic change of the impurity behavior. This doesn't mean the penetration depth of the impurity is not important. It should be pointed out that there is a strong difference between the tracers deposited inside the plasma and the intrinsic impurities entering through the plasma periphery in the high density case. The precise location (and width) discriminating the difference is an interested point to be investigated in future.

4. Discussion

First of all, we would like to mention about the change of the $Z_{\rm eff}$ value due to the TESPEL injection. $Z_{\rm eff}$ is defined as follows:

$$Z_{\rm eff} = \frac{\sum_I n_I Z_I^2}{\sum_I n_I Z_I} = \frac{\sum_I n_I Z_I^2}{n_{\rm e}},$$

where I denotes the ion species. Following this definition, the increase of $Z_{\rm eff}$, $\Delta Z_{\rm eff}$ due to the carbon contained in the TESPEL is 0.3 in average over the whole plasma in the medium density case, and 0.2 in the high density case. As for the tracers, the dominant charge state is helium-like at most in the present temperature range. For explaining this, the temporal evolution of (a) Co^{26+} (H-like charge state) and (b) Co^{27+} (fully ionized charge state) calculated by STRAHL in the high density case is shown in Fig. 12. Comparing Fig. 12 with Fig. 3, it is easily understandable, that is, the Co^{26+} ion density is less by a factor of about 300 than the Co^{25+} ion density, and the Co^{27+} ion density

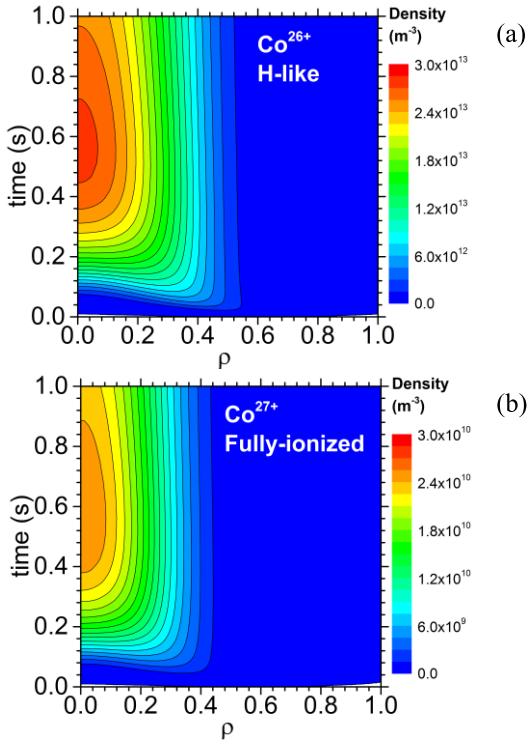

Fig. 12 The temporal evolution of (a) H-like and (b) fully ionized charge states of Co calculated by STRAHL in the high density case.

is less by a factor of about 3×10^5 than the Co^{25+} ion density. Taking this point, $\Delta Z_{\rm eff}$ due to the carbon and all the tracers is 0.8 for the medium density case, and 0.4 for the high density case. The measurement of the $Z_{\rm eff}$ at LHD [14] shows $Z_{\rm eff}=2$ for $n_{\rm e}(0)=4\times10^{19}\,{\rm m}^{-3}$ at $\rho=0$ and $n_{\rm e}=4\times10^{19}\,{\rm m}^{-3}$ at $\rho=0.9$ (Fig. 7 of [14]), and $Z_{\rm eff}=1.5$ for $n_{\rm e}=5\times10^{19}\,{\rm m}^{-3}$ at $\rho=0$ and $n_{\rm e}=9\times10^{19}\,{\rm m}^{-3}$ at $\rho=0.9$ (Fig. 9 of [14]). Here we take these numbers as representative for the medium and high density cases, respectively. The spatial profiles of those $Z_{\rm eff}$ are rather flat. The post-TESPEL $Z_{\rm eff}$ for the medium density case increases from 2 to 2.6. Thus, $\Delta Z_{\rm eff}/Z_{\rm eff}=0.3$. In the high density case, the post-TESPEL $Z_{\rm eff}$ increases from 1.5 to 1.9. Thus, $\Delta Z_{\rm eff}/Z_{\rm eff}=0.3$. From these calculations, the change of $Z_{\rm eff}$ itself is not negligible. On the other hand, the change of the electron temperature and the stored energy due to the TESPEL injection is negligible as stated in the previous paper [5]. The possible effect due to the increase of $Z_{\rm eff}$ may be, for example, the increase of the collisionality. So, we should say the present result about the impurity behavior is applicable within the $Z_{\rm eff}$ increase of about 30%.

The intrinsic impurities were observed to be accumulated in case of the medium density in the previous results by Nakamura *et al.* [9]. The present results show that the Kα and Li-like line emissions from the tracers deposited locally in the plasma for a short time (typically order of 50 μs) decay in time of ~500 ms. And, this decay feature is well simulated by STRAHL. Thus, it indicates that the phenomenon of the accumulation of the intrinsic impurities is due to the continuous source of the intrinsic impurities from the plasma periphery. When the impurity source supplies the impurity quantity more into the plasma core than the loss of impurity from the plasma core region, then the impurity is accumulated. In fact, the Kα and Li-like line emissions from the intrinsic impurity, Fe are kept almost constant or increase in the medium density case in contrast to those of the tracers. On the other hand, in the high density case with relatively low $T_{\rm e}$, the intrinsic impurity was observed not to be accumulated in the previous results. One might consider it is inconsistent with the present results showing that the tracers are kept for a long time in the high density regime. However, these indicate clearly the importance of the initial deposition location of the impurity for determining the impurity transport property. When the intrinsic impurity is coming from the plasma periphery, then such impurity cannot enter into the plasma core. The characteristics of such suppression of the intrinsic impurities will be described in detail in the separate paper. In contrast to the medium density case, when the impurity is deposited in the plasma (say at $\rho\sim0.6$ - 0.7) in the high density case, the impurity is kept for a long time. From the viewpoint that the influx of the intrinsic impurities is suppressed, the previous and present results are consistent. The present results elucidated the new aspect that the direct deposition of the impurity inside the plasma causes a long confinement time of impurities in the high density case. Such new finding is owing to the advantage of TESPEL together with the simultaneous measurement of the tracers and intrinsic impurities. STRAHL calculation showed the diffusion coefficient in case of the high density is at least by a factor of 2 smaller than that of the medium density case, if the convection velocity is not changed. For more precise determination of the diffusion coefficient or confinement time, the experiment with longer duration will be necessary. The property of the long confinement time of the impurity in the high density case suggests that impurities coming in a flake form may remain for a long time, and also that the He ash produced inside of the plasma may remain also for a long time in a future reactor machine.

5. Conclusion

The impurity behaviors in the plasma core and periphery have been studied by a triple-tracer TESPEL injection. So far it has been found that the impurity transport property in the medium density is different from that in the high density case. It is found that the STRAHL simulation is useful for describing the triple tracer experimental results of the impurity transport with ionization and recombination. The experimental data are compared with the STRAHL calculation assuming the impurity diffusion coefficient D (spatially constant) and convection velocity V (inward convection only in the plasma periphery). With D

of 0.1 m^2/s in case of the high density and 0.2 m^2/s in case of the medium density, the simulation data are fitted relatively well with the experimental one. For more detailed comparison, the diagnostics with higher spatial and temporal resolutions are needed which is under preparation.

Acknowledgements

This work is supported by a Grant-in-Aid for Scientific Research (B) (No. 19340179 and 23360415) from JSPS Japan and budgetary Grant-in-Aid of NIFS09ULHH012, NIFS10ULHH012 and NIFS11ULHH012 from NIFS.

[1] S. Sudo, J. Plasma Fusion Res. **69**, 1349 (1993).
[2] S. Sudo *et al.*, Plasma Phys. Control. Fusion **44**, 129 (2002).
[3] S. Sudo *et al.*, Plasma Phys. Control. Fusion **45**, 1127 (2003).
[4] S. Sudo and N. Tamura, Rev. Sci. Instrum. **83**, 023503 (2012).
[5] S. Sudo, N. Tamura *et al.*, Nucl. Fusion **52**, 063012 (2012).
[6] K. Behringer "Description of the impurity transport code STRAHL" JET-R(87)08, JET Joint Undertaking, Culham.
[7] K. Narihara *et al.*, Rev. Sci. Instrum. **72**, 1122 (2001).
[8] K. Kawahata *et al.*, Rev. Sci. Instrum. **70**, 707 (1999).
[9] Y. Nakamura *et al.*, Nucl. Fusion **43**, 219 (2003).
[10] S. Muto *et al.*, Rev. Sci. Instrum. **72**, 1206 (2001).
[11] J.L. Schwob, A.W. Wouters, S. Suckewer and M. Finkenthal, Rev. Sci. Instrum. **58**, 1601 (1987).
[12] H.P. Summers "The ADAS User Manual", version 2.6 (2004). http://www.adas.ac.uk
[13] K. Ida *et al.*, Nucl. Fusion **44**, 290 (2004).
[14] H.Y. Zhou, S. Morita, M. Goto *et al.*, Plasma Fusion Res. **5**, S1021 (2010).